Selectable-FSR 10-GHz Granularity WDM Superchannel Filter in a Reconfigurable Photonic Integrated Circuit

Yiwei Xie, Zihan Geng, Deming Kong, *Member, IEEE*, Leimeng Zhuang, *Senior Member, IEEE*, and Arthur J. Lowery, *Fellow, IEEE*

***Abstract*—We present a 10-GHz granularity reconfigurable WDM superchannel filter in a photonic integrated circuit. The filter uses a ring-resonator-assisted tapped-delay-line topology. An example configuration with two ring resonators and four tapped delay lines provides a spectral filter with a flat-top passband, a roll-off factor of 8%, a tunable central wavelength, and a selectable free spectral range, i.e., 2× or 4× the 3-dB passband bandwidth. The device was fabricated in a silicon nitride (Si_3N_4/SiO_2) waveguide with a chip area of 0.36 cm^2 and has a fiber-to-fiber insertion loss of 5 dB. We experimentally demonstrate the filter for selecting a subchannel from a WDM superchannel comprising 10-GHz subchannels with 10% and zero guard bands. Owing to the infinite impulse responses of ring resonators, this filter requires a significantly smaller area and fewer tuning elements compared with designs based on only tapped-delay-line finite-impulse-response filters. This paper contributes to the creation of chip-scale all-optical WDM superchannel transceivers and reconfigurable optical add/drop multiplexers (ROADMs).**

***Index Terms*—Fast Fourier transform, fiber communications, Nyquist filter, optical signal processing, photonic integrated circuit, transceiver, waveguide device, WDM.**

I. Introduction

NEXT-GENERATION high-capacity optical communication networks would benefit from multi-carrier techniques, such as orthogonal frequency division multiplexing (OFDM) and wavelength division multiplexed (WDM) superchannels [1]–[4], as they support high spectral efficiencies by allowing carriers to be spaced at or close to signal baud rate. In terms of flexible channel generation and management, WDM superchannels are of particular interest because the shaping and (de)multiplexing of their subchannels can be implemented in the optical domain using optical filters [5], [6]. In effect, this could significantly reduce the workload of digital signal processing and of the signal conversion between electrical and optical domains, offering advantages of low power consumption, latency and cost.

Optical subchannel selections are a key function for the implementation of WDM superchannel receivers, which should be able to select a particular subchannel with minimum spectral distortion and crosstalk [7]–[11]. Free-space optics is able to provide very flexible filter characteristics; however, it is typically bulky and has limited spectral resolution [12], [13]. Photonic integrated circuits (PICs) could offer advantages with respect to size, weight, power consumption, stability, cost, and spectral resolution [14]–[25]. In terms of signal processing, most PIC WDM filter topologies implement finite impulse response (FIR) filters, including arrayed waveguide grating routers [26]–[28] and coupler-based tapped-delay-line filters [29]–[31]. Although they offer tuning flexibility, these filters have a trade-off between performance and complexity. In particular, for WDM superchannel applications, tens to hundreds of delay lines, with lengths of tens of centimeters, would be required to achieve a filter passband roll-off factor $<10\%$ and a frequency resolution in the order of sub-GHz [32], [33]. This raises challenges for device fabrication with respect to waveguide uniformity and loss, which have a significant impact on the filter's bandwidth and shape, together with the risk of lower yield per wafer due to the large chip size. In comparison, PIC filter topologies based on infinite impulse response (IIR) filters, e.g., using ring resonators, have the advantages of smaller size and lower complexity, as IIR filters provide long delays by means of path reuse [34]–[37]. However, most prior works on such filters were targeted at coarse wavelength filtering and/or have limited functional reconfigurability.

In this work, we investigate a solution for selecting subchannel from WDM superchannel signals comprising 10-GHz subchannels with 10% and zero guard bands. We experimentally demonstrate a photonic integrated circuit as a highly selective filter in the receiver. Our filter topology is derived from a part of previous theoretical study of a WDM superchannel

Manuscript received October 27, 2017; revised January 29, 2018 and March 21, 2018; accepted March 22, 2018. Date of publication March 26, 2018; date of current version May 11, 2018. This work was supported by the Australian Research Council Laureate Fellowship under Grant FL13010041. *(Corresponding author: Leimeng Zhuang.)*

Y. Xie and L. Zhuang are with the Electro-Photonics Laboratory, Department of Electrical and Computer Systems Engineering, Monash University, Melbourne, Vic 3800, Australia (e-mail: yiwei.xie@monash.edu; leimeng.zhuang@ieee.org).

Z. Geng, D. Kong, and A. J. Lowery are with the Electro-Photonics Laboratory, Department of Electrical and Computer Systems Engineering, Monash University, Melbourne, Vic 3800, Australia, and also with the Centre for Ultrahigh-bandwidth Devices for Optical Systems, Monash University, Melbourne, VIC, 3800, Australia (e-mail: Zihan.Geng@monash.edu; deming.kong@monash.edu; arthur.lowery@monash.edu).

Color versions of one or more of the figures in this paper are available online at http://ieeexplore.ieee.org.

Digital Object Identifier 10.1109/JLT.2018.2819687

demultiplexer [36], which uses ring resonator-assisted tapped delay lines (RATDL), that offer sharp passband roll-off for a relatively simple circuit. An exemplary configuration using two ring resonators (RRs) and four tapped delay lines provides a spectral filter with a flat-top passband, a roll-off factor of 8%, a tunable operation wavelength, and a selectable free spectral range (FSR), i.e., 2× or 4× the 3-dB passband bandwidth. For a first experimental verification, we had such a device fabricated in a silicon nitride (Si_3N_4/SiO_2) waveguide [38]–[40], with a chip area of 0.36 cm^2 and a fiber-to-fiber insertion loss of 5 dB. Using this chip in a 2-stage filtering setup, we successfully demonstrated the selection of a subchannel of WDM superchannel comprising 10-GHz subchannels with 10% and zero guard bands.

The remainder of the paper is organized as follows: Section II explains the device principle in terms of signal processing terminology; Section III shows the chip layout and characterization results. Section IV experimentally demonstrates the subchannel selection function with different settings of WDM superchannel; and Section V presents the conclusions.

II. Device Principle

A. Signal Processing Principle

Fig. 1 shows the signal processing principle of our filter designs with different FSR-passband ratios (FPRs), i.e., Fig. 1(a) with FPR $=$ 2 and Fig. 1(b) with FPR $= N$. As explained in prior work [36], [41], the filter in Fig. 1(a) uses a typical topology for implementing a Chebyshev Type II filter, which comprises a 2-tap delay line filter with each path loaded with a number of recursive filters. In principle, all of recursive filters should be of the same delay equal to twice the delay difference between the two paths, Δt. Besides, the number of recursive filters in the shorter path (Path 1), *X*, and that in the longer path (path 2), *Y*, should meet the condition of $X = Y$, or $X = Y - 1$. Satisfying this condition implements a *M*th-order ($M = 2 \cdot (X + Y) + 1$) filter with a flat-top passband, a roll-off factor depending on *M*, and a FPR $=$ 2 [42].

The filter in Fig. 1(b) is an evolution of that in Fig. 1(a), where each of the two delay paths is replaced by a sub-FIR filter. Here, both sub-FIR filters are tapped-delay-line filters with *N*/2 taps, with one having linearly incremental delay lines from 0 to (*N*/2-1)·Δt, whereas the other has delays from (*N*/2)·Δt to (*N*-1)·Δt. The outputs of the sub-FIR filters are fed to the recursive filters for flat-top passband shaping [36]. When *N* is a power of 2 and the delay of the recursive filters is changed to $N\Delta t$, the condition to implement Chebyshev Type II filter still holds [36]; the sub-FIR filters delays are switched in and out of circuit, so that the FPR can be changed.

B. Filter Transfer Function

The transfer function of the *N*-tap delay line filter is given by [42]:

$$H_{TDL}(z) = \sum_{n=0}^{N-1} \alpha_n z^{-n} \tag{1}$$

where α_n is the tap complex coefficient, $z^{-1} = \exp(-\mathrm{j}2\pi f \cdot \Delta t)$, f the frequency, and Δt the incremental delay, which determines the device FSR by $f_{\mathrm{FSR}} = 1/\Delta t$.

The transfer function of the recursive filter is given by [42]

$$H_{RE}(z) = \frac{\sqrt{1-\eta} - e^{-\mathrm{j}\theta} \cdot z^{-N}}{1 - e^{-\mathrm{j}\theta} \cdot z^{-N} \cdot \sqrt{1-\eta}} \tag{2}$$

where η is the coupling ratio and θ is the phase shift of the recursive filter. When combining Eq. (1) and Eq. (2), the complete transfer function from the input to the output is

$$\begin{aligned} H_{TDL-RE}(z) &= H_{TDL-RE\_1}(z) + H_{TDL-RE\_2}(z) \\ &= H_{TDL\_1}(z)H_{RE\_1}(z) + H_{TDL\_2}(z)H_{RE\_2}(z) \\ &= \left(\sum_{n=0}^{N/2-1} \alpha_n z^{-n} \right) \\ &\quad \times \left(\prod_{x=1}^{X} \frac{\sqrt{1-\eta_{L,x}} - e^{-\mathrm{j}\theta_{L,x}} \cdot z^{-N}}{1 - e^{-\mathrm{j}\theta_{L,x}} \cdot z^{-N} \cdot \sqrt{1-\eta_{L,x}}} \right) \\ &\quad + \left(\sum_{n=N/2}^{N-1} \alpha_n z^{-n} \right) \\ &\quad \times \left(\prod_{y=1}^{Y} \frac{\sqrt{1-\eta_{U,y}} - e^{-\mathrm{j}\theta y} \cdot z^{-N}}{1 - e^{-\mathrm{j}\theta_{U,y}} \cdot z^{-N} \cdot \sqrt{1-\eta_{U,y}}} \right) \end{aligned} \tag{3}$$

where η_L, θ_L, are the optical power coupling coefficient and optical phase shift of the recursive filters in Path 1, and η_U, θ_U in Path 2.

C. Photonic Integrated Circuit Design

Fig. 2(a) shows the schematics of the PIC implementation of the proposed filter using RATDL topology. The sub-FIR filters in Fig. 1(b) can be constructed using binary-tree coupler arrays and delay lines, this structure offers design flexibility and easy incorporation of tuning elements [42], [43]. The recursive filters can be implemented using simple-structured side-coupled RRs [36], [42]. In our design, the binary-tree-structured coupler array is implemented using 2 × 2 tunable Mach-Zehnder couplers (MZCs) whose coupling coefficients are set by tunable phase shifters in their arms. Dedicated tunable phase shifters are included in the delay lines. The incorporation of these tuning elements allows for full control of both the amplitude and phase of each tap coefficient, α_n.

The tuning elements enable the filter to be configured to have different passband shapes. When the RRs are decoupled ($\eta_U = \eta_L = 0$), the circuit reduces to an *N*-tap delay line filter. When the RRs are coupled (η_U, $\eta_L \neq 0$), the circuit can implement a WDM superchannel filter. The theoretical filter shapes are shown in Fig. 2(b)–(d). Fig. 2(b) demonstrates the filter shape with $N = 2$, 4, and 8, when the power coupling coefficients of RRs, η, are set to 0 and all α_n are set with equal values. The filters have sinc-like shapes, with the spectral width depending on the number of delay lines, *N*. Fig. 2(c) shows the 5th-order

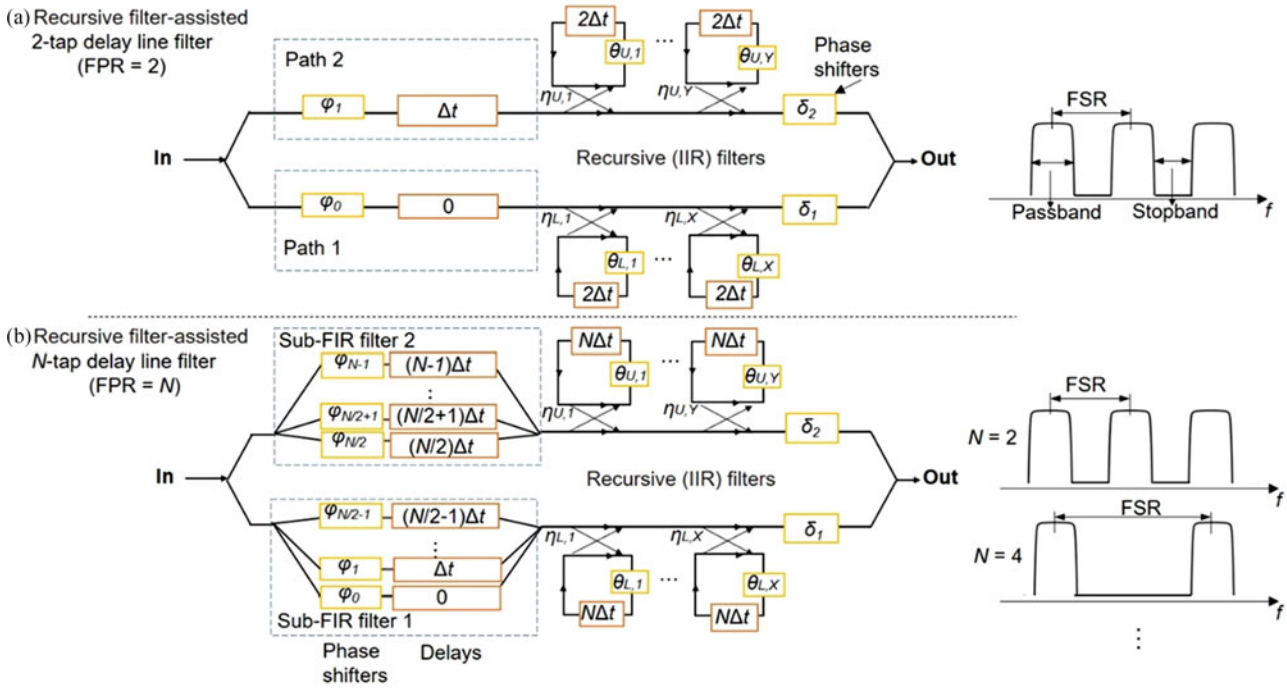

Fig. 1. Illustration of signal processing principle of: (a) recursive filter-assisted 2-tap delay line filter, (b) programmable recursive filter-assisted *N*-tap delay line filter.

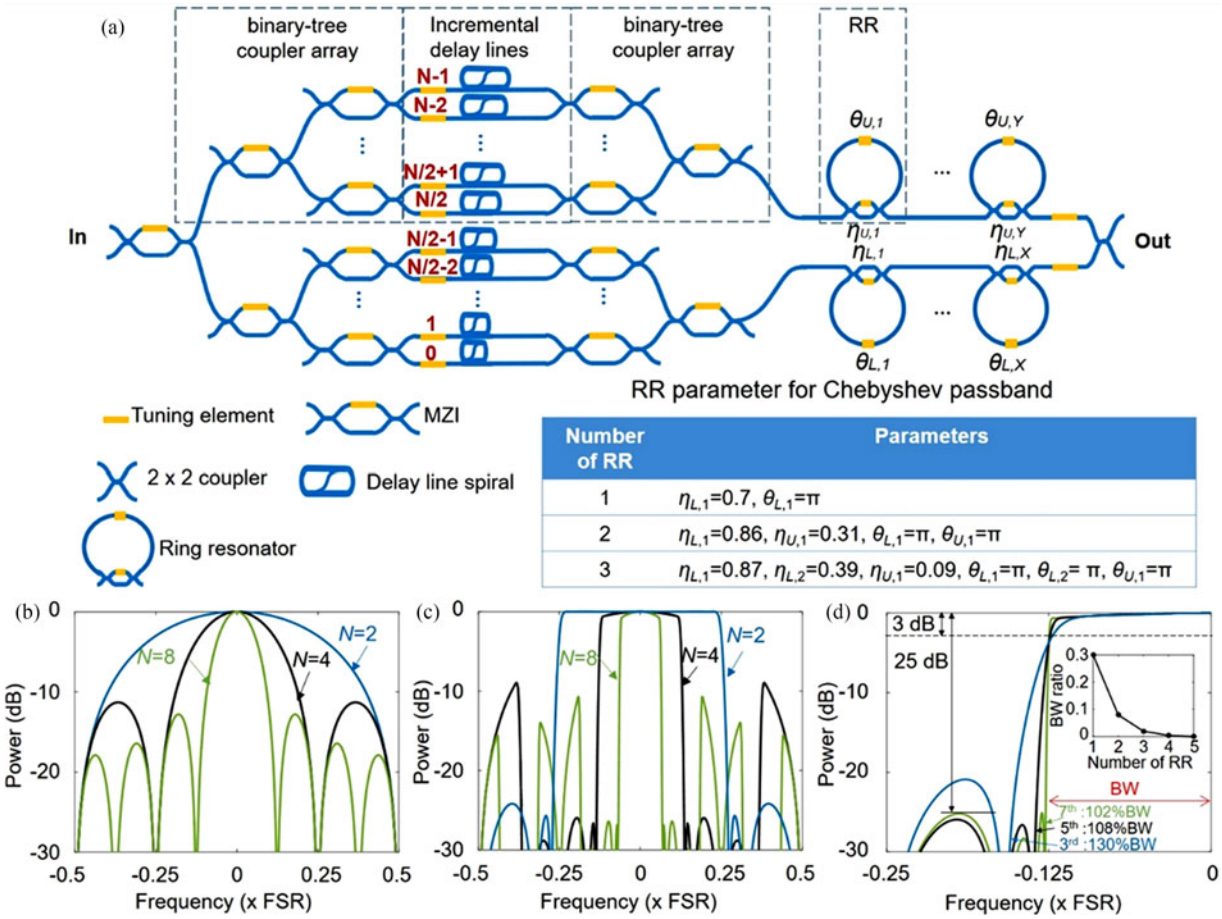

Number of RR	Parameters
1	$\eta_{L,1}$=0.7, $\theta_{L,1}$=π
2	$\eta_{L,1}$=0.86, $\eta_{U,1}$=0.31, $\theta_{L,1}$=π, $\theta_{U,1}$=π
3	$\eta_{L,1}$=0.87, $\eta_{L,2}$=0.39, $\eta_{U,1}$=0.09, $\theta_{L,1}$=π, $\theta_{L,2}$= π, $\theta_{U,1}$=π

Fig. 2. (a) Implementation of the *N*-tap (*X*+*Y*)-ring resonators-assisted tapped-delay line filter. Filter frequency response measurements: (b) the tapped-delay line filter with $N = 2, 4, 8$ without RRs; (c) the optimum setting of the 5th-order RATDL filter with $N = 2, 4, 8$; (d) 3rd-(blue), 5th- (black), 7th-order (green) RATDL filter (Inset table: RR parameters for Chebyshev passband, inset picture in Fig. 2(d): 25-dB passband ratio with respect to the number of rings, BW: Bandwidth).

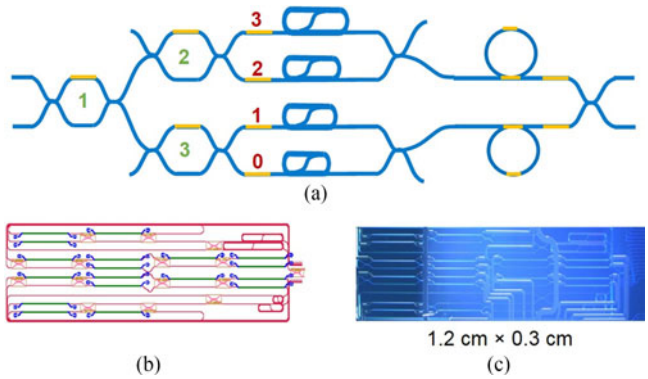

Fig. 3. (a) Schematic of the 5th-order RATDL filter with $N = 4$; (b) chip layout; (c) a photo of the fabricated chip.

Chebyshev filter shapes in association with different number of *N*, where two RRs are used, and their parameters are shown in the inset of Fig. 2. In this case, the filter provides near-rectangular passbands, and the corresponding FPRs equal to the number of *N*. Fig. 2(d) shows the filter shapes of 3rd-, 5th-, and 7th-order Chebyshev passbands (in accordance with the use of 1, 2, and 3 RRs) in association with $N = 4$. For the 5th-order case, the transition bands (suppression from -3 dB to -25 dB) are characterized by a roll-off factor of 8%. In terms of WDM superchannel multiplexing, such a passband shape would enable very dense multiplexing, e.g., Nyquist-spaced multiplexing [6], [36]. In principle, further sharpening of the transition bands is still possible by increasing the number of RRs; the inset in Fig. 2(d) shows the passband roll-off factors as a function of the number of RRs. However, this requires the added RRs to operate with coupling coefficients approaching zero [42], which raises challenges for device fabrication and control. In practice, both roll-off factor and implementation simplicity should be considered for the choice of the number of RRs in the circuit [6], [36].

III. Chip Design and Characterization

We designed a proof-of-concept device, which was fabricated using a Si_3N_4/SiO_2 waveguide (TriPleX) technology [38], [39], as shown in Fig. 3(a). This comprises four tapped delay lines and two RRs. The waveguide uses a "double-stripe" geometry [44] and has a group index of 1.71 and wavelength dependency of 2×10^{-5} /nm. It supports a single mode at 1550 nm and is optimized for light coupling with TE polarization. The delay interval of the tapped delay lines Δt is designed to be 25 ps, corresponding to a FSR of 40 GHz. For simplicity, the input coupler arrays of the sub-FIR filters are implemented using tunable MZCs, whereas the output coupler using 3-dB directional couplers instead. The tunable phase shifters are implemented thermo-optically using chromium heaters with a power consumption of 0.25 W/π. The total power consumption of the proposed filter with optimum setting is around 3 W. The RR roundtrip delay is 100 ps, giving a passband bandwidth of 10 GHz. Different FPRs of the RATDL filter can be obtained via changing the FSR of the filter by setting some tap complex coefficients $a_n = 0$.

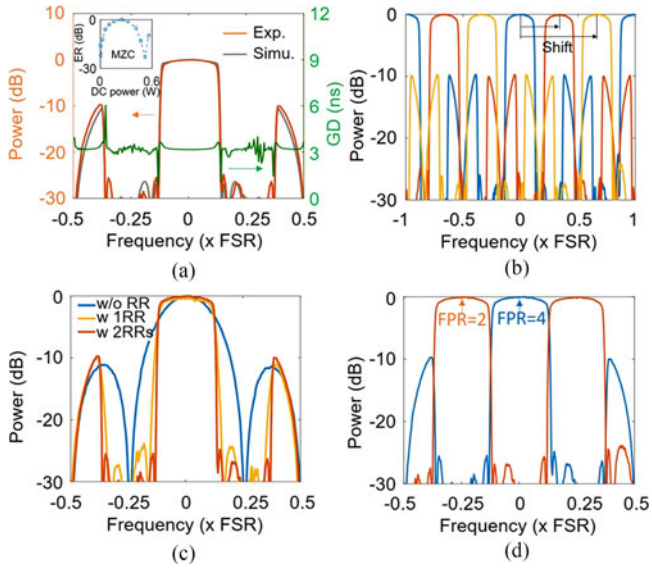

Fig. 4. Filter frequency response and GD measurements: (a) a comparison between measurement and calculation (using MATLAB); demonstrations of passband bandwidth variation with respect to (b) passband frequency shifting, (c) the number of rings, and (d) variation of filter's FPR. (Inset in Fig. 4(a): the ER of the MZC vs DC power.)

The chip layout is shown in Fig. 3(b). Parallel heaters are placed with a minimum spacing of 300 μm, to reduce the thermal crosstalk and guarantee performance uniformity between them. All building blocks are folded with bend radii of 150 μm, to reduce chip area. This structure minimizes the circuit complexity and heat dissipation compared with designs using a parallel array of couplers, while guaranteeing full control of both amplitude and phase of each optical path.

The fabricated chip is shown in Fig. 3(c), with an area of 0.36 cm^2. The chip is fully packaged with all of the heaters are wire-bonded to a carrier printed circuit board and optical I/Os are pigtailed with polarization-maintaining fibers. The total insertion loss of the packaged chip is 5 dB, which includes two fiber-chip interfaces and on-chip losses.

Fig. 4 shows a number of measured filter responses with different parameters as in the inset of Fig. 2. A LUNA OVA5000 (0.15-MHz resolution) was used to measure the responses. The LUNA measurements were single polarization. The circuit characterization and configuration were performed manually. The settings of the tuning elements that gave particular filter responses were identified and recorded. The manual process was to try to isolate the responses of some sections of the circuit while adjusting others (usually the simplest first). The isolated sections were then engaged one-by-one in the later stages of configuration.

For this particular circuit, the configuration steps are as follows. (Step 1) Exclude the effects of RRs by setting their couplers to zero cross-coupling. This status can be identified when the overall frequency response is not affected by the ring resonators; in this situation the circuit reduces to an FIR filter with 4 delay arms. (Step 2) Adjust the couplers in the input splitter array until the circuit impulse response measured with a fast oscilloscope and pulses source has the desired form, e.g., an

impulse response of [1, 1, 1, 1] for a 4-tap FIR filter or pattern of [1, 0, 1, 0] for a 2-tap FIR filter. (Step 3) Adjust the phase shifters in the delay arms until the overall frequency response shows a symmetric sinc shape with its center frequency aligned to the desired value. (Step 4) Couple the ring resonator on the side of the shorter delay arms back in. Adjust its coupler and phase shifter until the filter passband has a rectangular response, and the stopband has an overall extinction larger than 25 dB and 3 nulls. (Step 5) Couple the second ring resonator back in. Adjust its coupler and phase shifter until the filter passband shows improved selectivity, and the stopband has an overall extinction larger than 25 dB and 5 nulls.

Fig. 4(a) shows the filter response and group delay (GD) with the optimum setting (the parameters are shown in Table 1). The measurement is in good agreement with theoretical results [using (3)] with a relative error of 6%, showing a good accuracy of the circuit design and fabrication. The slight deviation from the ideal result is due to the limited extinction ratio (ER) of the MZC (23 dB), as shown in the inset of Fig. 4(a). The near-rectangular passband has a flat top with bandwidth of 10 GHz, and a 25-dB bandwidth of 10.8 GHz. Fig. 4(a) also shows that the filter response has GD variation at the edge of passband, but is almost the same over most of the passband. Fig. 4(b) demonstrates that the center frequency of the passband can be tuned while retaining the passband shape, by adding constant incremental phase shifts across all delay lines. Fig. 4(c) and (d) demonstrate changing the passband shape and FPR. This was performed by varying the amplitude coefficients of the filter and the parameters of RRs. In Fig. 4(c), three filter shapes are shown, i.e., a sinc-like shape, a 3rd-order and a 5th-order Chebyshev shape. To get these results, all α_n are set with equal values, and the number of RRs coupled to the circuit are 0, 1, 2, respectively. Here, this filter passband has a sharp roll-off, rolling down more rapid than a RR engaged filter. This results from the selectivity enhancement due to the interference of the MZI, where a slower phase change converts into faster intensity change [45]. In Fig. 4(d), two filter shapes are shown with different FPRs, i.e., FPR $= 2$ and FPR $= 4$. This is achieved by changing the tap amplitude coefficients, for FPR $= 2$, α_0, $\alpha_2 = 0$ (or α_1, $\alpha_3 = 0$), so that the circuit has an equivalent $N = 2$; for FPR $= 4$, all α_n are set to be non-zero, resulting in $N = 4$.

These results verify the full programmability of the filter. In particular, the capability of defining both the passband shift and the FPR are the key for Nyquist-WDM (N-WDM) reception, where the filter passbands select the desired frequency channels and suppress the undesired ones.

IV. System Experiment Results

To test the performance of the device in a system, an 80-GHz bandwidth, OOK-encoded N-WDM superchannel was generated, as shown in Fig. 5. Eight channels were shaped to be OOK-Nyquist signals at a symbol rate of 10 Gbaud. The transmitter consists of two arrays of external cavity lasers (ECLs), two Mach-Zehnder modulators (MZMs) and a coupler to form de-correlated N-WDM superchannel.

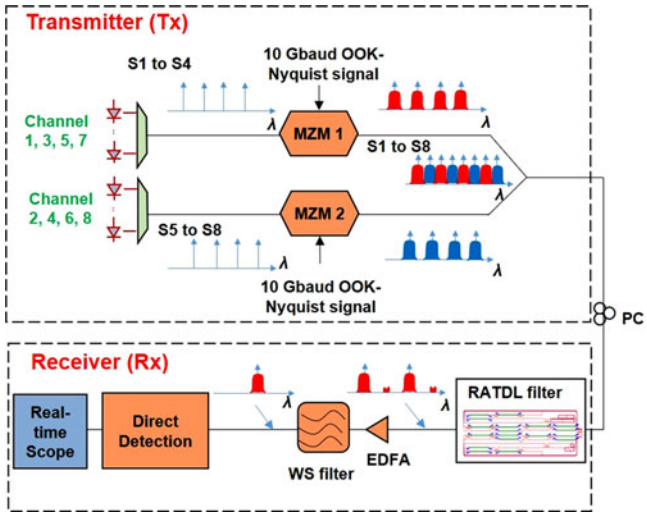

Fig. 5. System experiment setups for Nyquist superchannel demultiplexing system. (WS: WaveShaper, EDFA: erbium-doped fiber amplifier, PC: polarization controller.)

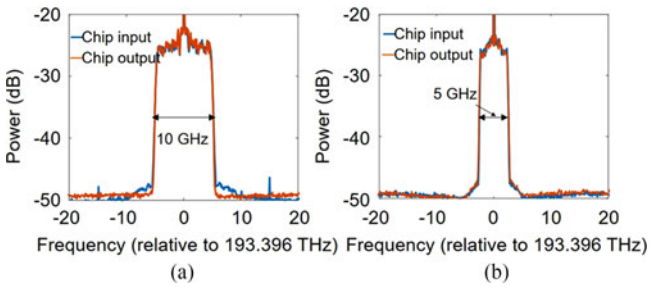

Fig. 6. Spectra of a single Nyquist signal before and after the chip when the rate of the signal is (a) 10 Gbaud and (b) 5 Gbaud.

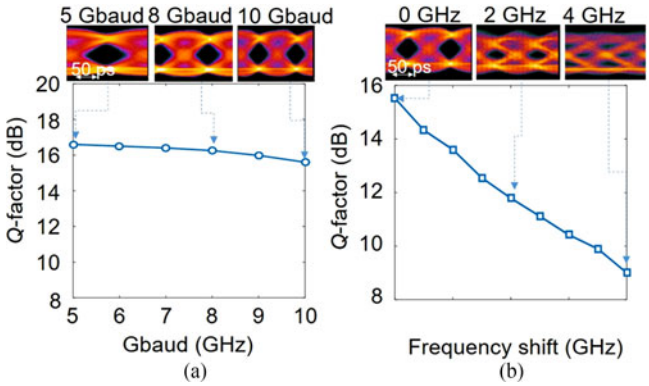

Fig. 7. Q factor measurements for single Nyquist channel with respect to (a) the rate of the signals with equal noise power for each OSNR (Inset: eye diagrams) (b) frequency shift of the input ECL when the OSNR is 20 dB.

Each optical source array contains four independent ECLs, which are spaced 20-GHz apart, and are combined together using a polarization maintaining 1×4 coupler before modulation with 10-GHz bandwidth intensity modulators, driven by wavewforms generated from a 60-GSa/s arbitrary waveform generator (AWG). The AWG output is a Nyquist signal with stopband suppression ratio of 25 dB. This produces 'odd' and 'even' OOK-Nyquist subchannels. The modulated signals are combined to generate Nyquist superchannel comprising eight

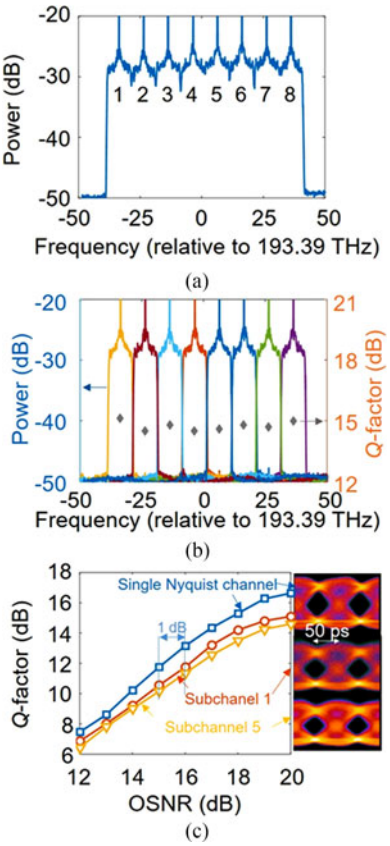

Fig. 8. N-WDM superchannel without guard band: (a) Spectrum of eight N-WDM superchannel. (b) Signal spectra and *Q*-factor measurement (OSNR = 20 dB) of all subchannels. (c) Measured *Q*-factor *vs.* OSNR for central subchannel (Subchannel 5) and edge subchannel (Subchannel 1) in N-WDM superchannel system, single Nyquist signal system is the reference (inset: Eye diagrams of the three cases when OSNR = 20 dB).

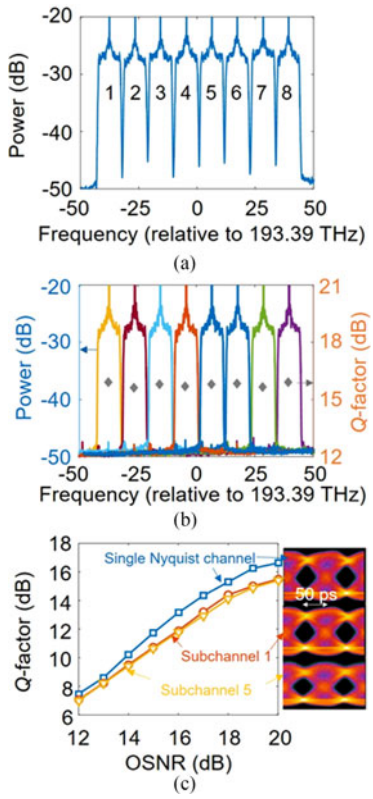

Fig. 9. N-WDM superchannel with 10% guard band: (a) Spectrum of eight N-WDM superchannel. (b) Signal spectra and *Q*-factor measurements (OSNR = 20 dB) of all sub-channels. (c) Measured Q *vs.* OSNR for central (Subchannel 5) and edge subchannel (Subchannel 1) in N-WDM system, single Nyquist signal system is the reference (Eye diagrams of the three cases when OSNR = 20 dB).

10-Gbaud OOK-modulated Nyquist signals. The odd and even subchannels are decorrelated. The modulators' output is noise loaded for the control of optical signal-to-noise ratio (OSNR).

A direct-detection receiver is used, comprising a 70-GHz photodetector (Finisar XPDV3120) and a 80-Gsa/s 28-GHz real-time oscilloscope (Agilent DSO-X 95004Q). The receiver uses the proposed filter for fine-resolution selection of the 10-GHz subchannels; a 20-GHz bandwidth filter (WaveShaper) removes the undesired passbands of the proposed filter.

A. *Single Nyquist-Channel Results*

Firstly, the performance of single Nyquist channel with ECL frequency drift and different signal rates was assessed. Only one ECL was used. Fig. 6(a) and (b) show the input and output spectra of the RATDL filter for 10-Gbaud and 5-Gbaud Nyquist signals, respectively. The input and output spectra are very similar. Fig. 7(a) shows the performance of output signal with respect to the transmitted signal rate at an OSNR of 20 dB (0.1 nm). For 10 Gbaud, the signal at the edge of the passband has different GD than other portion of signal in the centre of passband, as shown in Fig. 4(a); this results in a penalty of less than 1 dB. In Fig. 7(b), when the central frequency of the Nyquist signal is tuned away form the centre of filter passband, the performance decreases, as shown in the inset eye diagrams in Fig. 7(b).

B. *N-WDM Superchannel System Results*

We now demonstrate subchannel selection without guard band, using the setup in Fig. 5. This circuit was fabricated with a usable bandwidth of a few hundred GHz. Previous works using the same kind of waveguide with better fabrication accuracy have shown usable bandwidths in the order many THz [6]. Here, we focus on eight channels to prove the subchannel selection concept. Fig. 8(a) shows the spectrum of N-WDM superchannel before input into the RATDL filter. Fig. 8(b) shows the spectra of the selected Nyquist subchannels at the output of the WaveShaper (WS) filter. Each subchannel was successfully demultiplexed in-turn, and the *Q*-factors of the subchannels are similar. The outer subchannels (Subchannel 1 and 8) have slightly better performance than the central subchannels (Subchannels 2-7) because they have fewer neighbors, as shown in Fig. 8(b). Fig. 8(c) compares the back-to-back optical signal to noise ratio (OSNR) performance of a single Nyquist signal without the RATDL filter (as reference), with a demultiplexed outer subchannel (Subchannel 1), and a central subchannel (Subchannel 5) of Nyquist-WDM superchannel. The results show the subchannels have a 1-dB reduction in signal quality compared with the single Nyquist channel, due to the crosstalk

from neighboring subchannels and the GD of the RATDL filter. The central subchannels have less than 0.4-dB additional penalty compared with the outer subchannels in N-WDM system because of crosstalk. The eye diagram in Fig. 8(c) shows the performance of three cases when OSNR is 20 dB.

In N-WDM systems, a guard band is often introduced between the subchannels to reduce ICI. Fig. 9(a) shows the spectrum of N-WDM superchannel with 10% guard bands (11-GHz spacing). The measured Q-factors of the demultiplexed subchannels are very similar, as shown in Fig. 9(b). Fig. 9(c) plots the signal quality versus OSNR for the outer and central subchannels. The performance of both outer and central subchannels is similar, because the guard band reduces crosstalk.

V. Discussions and Conclusions

We have reported a new implementation of WDM- superchannel filter. The circuit is constructed using common PIC building blocks. The employment of tuning elements allows the filter's characteristics to be varied with respect to passband shape, central frequencies, FPR, and FSR. Using this chip in a 2-stage filtering setup, we have successfully demonstrated subchannel selection of N-WDM superchannel comprising 10-GHz subchannels with 10% and zero guard bands. The results of this work contribute to the creation of chip-scale all-optical WDM superchannel transceivers and ROADMs, underlining the potential of photonic integrated circuits for being a technology-enabling hardware platform for next-generation, high-capacity elastic optical communication networks. It is worth noting the waveguide used in this work only couples with the TE polarization. In case of dual-polarization signals, one possible solution is to split and combine two orthogonal polarizations off-chip and process each polarization individually using a chip. This, however, would incur issues like inter-polarization phase drifts, additional loss, and more complex control. Another possible solution is to use a waveguide that supports both polarizations and enable monolithic implementation of the processing functions. Silicon and indium phosphide platforms are possible options, but need further reductions in waveguide loss to be practical, particularly when delay path lengths of tens of centimeters are required on chip. Previous investigations of TriPleX also demonstrated waveguide geometries with a box-like shape which reduce the polarization sensitivity [46]. However, their increased sidewall roughness has a higher loss. For subchannel selection experiments, the current design requires additional coarse-step filter stage to perform complete subchannel selection due to the residual components at undesired subchannel frequencies. Future work will include multiple filter stages in one device.

References

[1] A. J. Lowery and L. B. Du, "Optical orthogonal division multiplexing for long haul optical communications: A review of the first five years," *Opt. Fiber Technol.*, vol. 17, no. 5, pp. 421–438, Oct. 2011.

[2] S. Shimizu, G. Cincotti, and N. Wada, "Demonstration and performance investigation of all-optical OFDM systems based on arrayed waveguide gratings," *Opt. Express*, vol. 20, no. 26, pp. B525–B534, Dec. 2012.

[3] I. Kang *et al.*, "Energy-efficient 0.26-Tb/s coherent-optical OFDM transmission using photonic-integrated all-optical discrete Fourier transform," *Opt. Express*, vol. 20, no. 2, pp. 896–904, Jan. 2012.

[4] Y. Yin, K. Wen, D. J. Geisler, R. Liu, and S. J. B. Yoo, "Dynamic on-demand defragmentation in flexible bandwidth elastic optical networks," *Opt. Express*, vol. 20, no. 2, pp. 1798–1804, Jan. 2012.

[5] A. Melloni and M. Martinelli, "Synthesis of direct-coupled-resonators bandpass filters for WDM systems," *J. Lightw. Technol.*, vol. 20, no. 2, pp. 296–303, Feb. 2002.

[6] L. Zhuang *et al.*, "Sub-GHz-resolution C-band Nyquist- filtering interleaver on a high-index-contrast photonic integrated circuit," *Opt. Express*, vol. 24, no. 6, pp. 5715–5727, Mar. 2016.

[7] T. Chiba, H. Arai, K. Ohira, H. Nonen, H. Okano, and H. Uetsuka, "Novel architecture of wavelength interleaving filter with Fourier transform-based MZIs," in *Proc. Opt. Fiber Commun. Conf.*, Anaheim, CA, USA, 2001, Paper WB5.

[8] C. Chen *et al.*, "Reconfigurable optical interleaver modules with tunable wavelength transfer matrix function using polymer photonics lightwave circuits," *Opt. Express*, vol. 22, no. 17, pp. 19895–19911, Aug. 2014.

[9] S. Cao *et al.*, "Interleaver technology: Comparisons and applications requirements," *J. Lightw. Technol.,* vol. 22, no. 1, pp. 281–289, Jan. 2004.

[10] C. Chen *et al.*, "Monolithic multi-functional integration of ROADM modules based on polymer photonic lightwave circuit," *Opt. Express*, vol. 22, no. 9, pp. 10716–10727, May 2014.

[11] L. Zong, H. Zhao, Z. Feng, and Y. Yan, "8 × 8 flexible wavelength cross-connect for CDC ROADM application," *Photon. Technol. Lett.*, vol. 27, no. 24, pp. 2603–2606, Dec. 2015.

[12] J. Schröder, L. B. Du, J. Carpenter, B. J. Eggleton, and A. J. Lowery, "All-optical OFDM with cyclic prefix insertion using flexible wavelength selective switch optical processing," *J. Lightw. Technol.*, vol. 32, no. 4, pp. 752–759, Feb. 2014.

[13] N. Nemoto *et al.*, "8 × 8 wavelength cross connect with add/drop ports integrated in spatial and planar optical circuit," in *Proc. Eur. Conf. Opt. Commun.*, Valencia, Spain, 2015, Paper Tu.3.5.1.

[14] W. Liu *et al.*, "A fully reconfigurable photonic integrated signal processor," *Nature Photon.*, vol. 10, no. 3, pp. 190–195, Mar. 2016.

[15] M. J. R Heck, J. F. Bauters, M. L. Davenport, D. T. Spencer, and J. E. Bowers, "Ultra-low loss waveguide platform and its integration with silicon photonics," *Laser Photon. Rev*., vol. 8, no. 5, pp. 667–686, Sep. 2014.

[16] L. Zhuang, C. G. H. Roeloffzen, M. Hoekman, K. J. Boller, and A. J. Lowery, "Programmable photonic signal processor chip for radiofrequency applications," *Optica*, vol. 2, no. 10, pp. 854–859, Oct. 2015.

[17] B. G. Saavedra *et al.*, "8-channel InP OFDM transmitter PIC with integrated optical Fourier transform," in *Proc. Eur. Conf. Opt. Commun.*, Dusseldorf, Germany, 2015, Paper PW.4.P1.

[18] B. Guan *et al.*, "CMOS compatible reconfigurable silicon photonic lattice filters using cascaded unit cells for RF-photonic processing," *J. Sel. Topics Quantum Electron.*, vol. 20, no. 4, pp. 359–368, Jul. 2014.

[19] D. J. Moss, R. Morandotti, A. L. Gaeta, and M. Lipson, "New CMOS-compatible platforms based on silicon nitride and Hydex for nonlinear optics," *Nature Photon.*, vol. 7, no. 8, pp. 597–607, Aug. 2013.

[20] L. Zhuang, "Flexible RF filter using a nonuniform SCISSOR," *Opt. Lett.*, vol. 41, no. 6, pp. 1118–21, Mar. 2016.

[21] M. H. Khan *et al.*, "Ultrabroad-bandwidth arbitrary radiofrequency waveform generation with a silicon photonic chip-based spectral shaper," *Nature Photon.*, vol. 4, no. 2, pp. 117–122, Feb. 2010.

[22] F. Morichetti, C. Ferrari, A. Canciamilla, and A. Melloni, "The first decade of coupled resonator optical waveguides: Bringing slow light to applications," *Laser Photon. Rev.*, vol. 6, no. 1, pp. 74–96, Jan. 2012.

[23] W. Bogaerts *et al.*, "Silicon microring resonators," *Laser Photon. Rev.*, vol. 6, no. 1, pp. 47–73, Jan. 2012.

[24] J. Capmany, I. Gasulla, and D. Pérez, "Microwave photonics: The programmable processor," *Nat. Photon.*, vol. 10, no. 1, pp. 6–8, Jan. 2016.

[25] Z. Geng *et al.*, "Photonic integrated circuit implementation of a sub-GHz-selectivity frequency comb filter for optical clock multiplication," *Opt. Express*, vol. 25, no. 22, pp. 27635–27645, Oct. 2017.

[26] M. K. Smit and C. Van Dam, "PHASAR-based WDM-devices: Principles, design and applications," *J. Sel. Topics Quantum Electron.*, vol. 2, no. 2, pp. 236–250, Jun. 1996.

[27] D. Dai, J. Wang, S. Chen, S. Wang, and S. He, "Monolithically integrated 64-channel silicon hybrid demultiplexer enabling simultaneous wavelength-and mode-division-multiplexing," *Laser Photon. Rev.*, vol. 9, no. 3, pp. 339–344, Mar. 2015.

[28] A. J. Metcalf *et al.*, "Integrated line-by-line optical pulse shaper for high-fidelity and rapidly reconfigurable RF-filtering," *Opt. Express*, vol. 24, no. 21, pp. 23925–23940, Oct. 2016.
[29] K. Takiguchi, M. Oguma, T. Shibata, and H. Takahashi, "Demultiplexer for optical orthogonal frequency-division multiplexing using an optical fast-Fourier-transform circuit," *Opt. Lett.*, vol. 34, no. 12, pp. 1828–1830, Jun. 2009.
[30] T. Goh, M. Itoh, H. Yamazaki, T. Saida, and T. Hashimoto, "Optical Nyquist-filtering multi/demultiplexer with PLC for 1-Tb/s class super-channel transceiver," in *Proc. Opt. Fiber Commun. Conf. Exhib.*, Los Angeles, CA, USA, 2015, paper Tu3A-5.
[31] F. Horst, W. M. Green, S. Assefa, S. M. Shank, Y. A. Vlasov, and B. J. Offrein, "Cascaded Mach-Zehnder wavelength filters in silicon photonics for low loss and flat pass-band WDM (de-) multiplexing," *Opt. Express*, vol. 21, no. 10, pp. 11652–11658, May 2013.
[32] N. Goldshtein *et al.*, "Fine resolution photonic spectral processor using a waveguide grating router with permanent phase trimming," *J. Lightw. Technol.*, vol. 34, no. 2, pp. 379–385, Jan. 2016.
[33] A. J. Lowery, Y. Xie, and C. Zhu, "Systems performance comparison of three all-optical generation schemes for quasi-Nyquist WDM," *Opt. Express*, vol. 23, no. 17, pp. 21706–21718, Aug. 2015.
[34] S. H. Jeong, S. Tanaka, T. Akiyama, S. Sekiguchi, Y. Tanaka, and K. Morito, "Flat-topped and low loss silicon-nanowire-type optical MUX/DeMUX employing multi-stage microring resonator assisted delayed Mach-Zehnder interferometers," *Opt. Express*, vol. 20, no. 23, pp. 26000–26011, Nov. 2012.
[35] P. Dong *et al.*, "GHz-bandwidth optical filters based on high-order silicon ring resonators," *Opt. Express*, vol. 18, no. 23, pp. 23784–23789, Nov. 2010.
[36] L. Zhuang *et al.*, "Nyquist-filtering (de) multiplexer using a ring resonator assisted interferometer circuit," *J. Lightw. Technol.*, vol. 34, no. 8, pp. 1732–1738, Apr. 2016.
[37] X. Jiang *et al.*, "Design and experimental demonstration of a compact silicon photonic interleaver based on an interfering loop with wide spectral range," *J. Lightw. Technol.*, vol. 35, no. 17, pp. 3765–3771, Sep. 2017.
[38] C. G. Roeloffzen *et al.*, "Low-loss Si3N4 TriPleX optical waveguides: Technology and applications overview," *J. Sel. Topics Quantum Electron.*, vol. 24, no. 4, Jul./Aug. 2018, Art. no. 4400321.
[39] C. G. H. Roeloffzen *et al.*, "Silicon nitride microwave photonic circuits," *Opt. Express*, vol. 21, no. 19, pp. 22937–22961, Sep. 2013.
[40] Y. Xie *et al.*, "Programmable optical processor chips: Towards photonic RF filters with DSP-level flexibility and MHz-band selectivity," *Nanophotonics*, vol. 7, no. 2, pp. 421–454, Oct. 2017.
[41] B. Corcoran *et al.*, "Multipass performance of a chip-enhanced WSS for Nyquist-WDM sub-band switching," *J. Lightw. Technol.*, vol. 34, no. 18, pp. 1824–1830, Apr. 2016.
[42] C. K. Madsen and J. H. Zhao, *Optical Filter Design and Analysis: A Signal Processing Approach*, Hoboken, NJ, USA: Wiley, 1999.
[43] M. S. Rasras *et al.*, "A programmable 8-bit optical correlator filter for optical bit pattern recognition," *Photon. Technol. Lett.*, vol. 20, no. 9, pp. 694–696, May 2008.
[44] L. Zhuang, D. Marpaung, M. Burla, W. Beeker, A. Leinse, and C. Roeloffzen, "Low-loss, high-index-contrast Si_3N_4/SiO_2 optical waveguides for optical delay lines in microwave photonics signal processing," *Opt. Express*, vol. 19, no. 23, pp. 23162–23170, Nov. 2011.
[45] L. Zhuang, M. Hoekman, R. M. Oldenbeuving, K. J. Boller, and C. G. Roeloffzen, "CRIT-alternative narrow-passband waveguide filter for microwave photonic signal processors," *Photon. Technol. Lett*, vol. 26, no. 10, pp. 1034–1037, May 2014.
[46] F. Morichetti *et al.*, "Box-shaped dielectric waveguides: A new concept in integrated optics?" *J. Lightw. Technol.*, vol. 25, no. 9, pp. 2579–2589, Sep. 2007.

Authors' biographies not available at the time of publication.